7 Impact of Packet Losses in Scalable Light Field Video Coding

Caroline Conti[§♀], Paulo Nunes[§♀], Luís Ducla Soares[§♀]

[§] ISCTE – Instituto Universitário de Lisboa (ISCTE-IUL), Av. das Forças Armadas,1649-026 Lisbon, Portugal

[♀] Instituto de Telecomunicações, Av. Rovisco Pais 1, 1049-001 Lisbon, Portugal (email: {caroline.conti, lds, paulo.nunes}@lx.it.pt)

Abstract

Light field imaging technology has been recently attracting the attention of the research community and the industry. However, to effectively transmit light field content to the end-user over error-prone networks – e.g., wireless networks or the Internet – error resilience techniques are required to mitigate the impact of data impairments in the user quality perception. In this context, this chapter analyzes the impact of packet losses when using a three-layer display scalable light field video coding architecture, which has been presented in Chapter 6. For this, a simple error concealment algorithm is used, which makes use of inter-layer redundancy between multiview and light field content and the inherent correlation of the light field content to estimate lost data. Furthermore, a study of the influence of 2D views generation parameters used in lower layers on the performance of the used error concealment algorithm is also presented.

7.1 Introduction

Light field is an imaging technology that has been attracting the attention of the research community and the industry for providing richer two-dimensional (2D) image capturing systems [1–3], single-camera 3D imaging and more immersive 3D viewing systems [4–6].

However, to progressively introduce this technology into the consumer market and to efficiently deliver light field content to end-users, a crucial requirement is backward compatibility with legacy 2D and 3D devices. Hence, to enable light field content to be delivered and presented on legacy displays, a scalable light field coding approach is required, where by decoding only the adequate subsets of the scalable bitstream, 2D or 3D compatible video decoders can present an appropriate version of the light field content.

Moreover, following the current forecasts indicating that three-quarters of the world's mobile data traffic will be video by 2020 [7], it should be envisaged to efficiently provide light field video services in such type of error prone environments. To guarantee this, error resilience techniques in the encoding and de-coding side are needed to mitigate the impact of data impairments in the user quality perception. The design of an appropriate error resilience technique typically considers the type of network (i.e., error characteristics of the network being used for transmission) and also the type of content (i.e., inherent characteristics of the content) being transmitted. In this sense, due to the different nature of acquisition system and, consequently, the different type of correlation in the light field content, when compared to the conventional 2D and 3D multiview contents, the set of factors which could affect the performance of an error control algorithm may also differ. Hence, it is essential to deeply understand the impact of packet losses in terms of decoding video quality for the specific case of light field content, notably when a scalable approach is used.

To the best of the authors' knowledge, the proposal of error resilience techniques suitable for light field content have been only addressed by the authors in [8]. In this context, this chapter aims to contribute to the discussion of this issue and presents a study of the influence of packet losses in scalable light field content coding. For this, the three-layer scalable light field video coding architecture presented in Chapter 6 (Section 6.4.1) is considered. Based on this coding architecture, a simple error concealment algorithm is proposed, which derives from the previously proposed inter-layer prediction method (Section 6.4.3.2) to estimate the lost data. Finally, an analysis of the influence of some meaningful parameters in the proposed coding architecture (e.g., 2D view generation parameters used in lower layers) on the performance of the used error concealment algorithm is also presented.

The remainder of this chapter is organized as follows: Section 7.2 briefly reviews the used scalable architecture for light field video coding, as well as the inter-layer prediction scheme, in order to better understand the proposed error concealment algorithm; Section 7.3 discusses some meaningful factors which affect the inter-layer prediction accuracy, and presents the proposed error concealment algorithm;

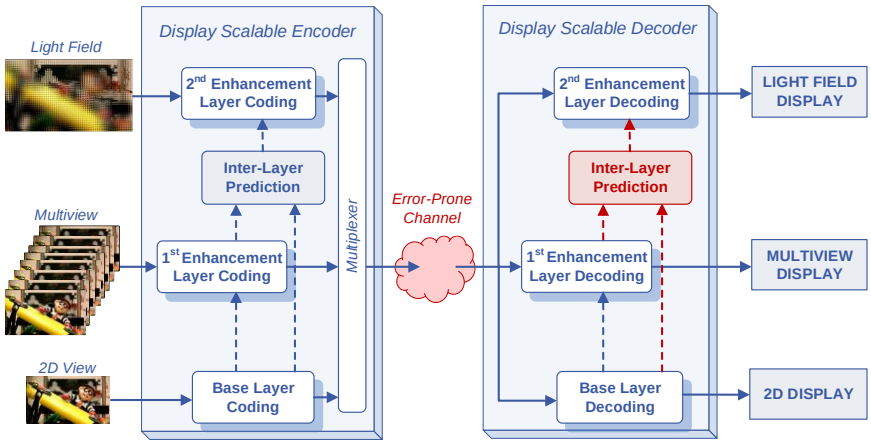

Fig. Error! Reference source not found.**.1** Display scalable light field coding architecture considered in this chapter for analyzing the impact of packet losses when transmitting in error-prone channels.

Section 7.4 presents the considered test conditions and studies the influence of packet losses on the accuracy of inter-layer prediction; and finally, Section 7.5 concludes the chapter.

7.2 Scalable Light Field Coding

The display scalable architecture for light field coding that has been presented in Section 6.4.1 is here considered (see Fig. 7.1). In this case, each layer of this scalable coding architecture represents a different level of display scalability:

- **Base Layer (2D)** – The base layer represents a single 2D view, which can be used to deliver a 2D version of the light field content to 2D displays devices.
- **First Enhancement Layer (Stereo or Multiview)** – This layer represents the necessary information to obtain an additional view (representing a stereo pair) or various additional views (representing multiview content). This is to allow stereo and autostereoscopic devices to play versions of the same light field content.
- **Second Enhancement Layer (Light Field)** – This layer represents the additional data needed to support full light field display.

For generating 2D views from the light field content to compose the content in the Base and First Enhancement Layers, two rendering algorithms, proposed in [9] and referred to as Basic Rendering and Weighted Blending, are here adopted. Essentially, there are two parameters that controls these algorithms: i) the patch size that controls the plane of focus in the generated view; and ii) the patch position that controls the viewing angle (i.e., the scene perspective).

High compression efficiency is still an important requirement for the scalable coding architecture adopted in this section. Therefore, an inter-layer prediction mode (see Fig. 7.1) is used to further improve the Second Enhancement Layer coding efficiency by removing redundancy between the light field content and its multiview version from the enhancement layer underneath. For this, an Inter-Layer (IL) reference picture is constructed by using the set of reconstructed 2D views obtained by decoding the bitstream in the lower layers. This IL reference picture can be then used as new a reference frame for employing an inter-layer compensated prediction when encoding the light field image. The process for constructing the IL reference picture can be basically divided into the following two steps (which are explained in detail in Section 6.4.1):

- **Patch Remapping** – The purpose of this step is to re-organize (remap) the texture samples (patches) from the reconstructed 2D views into its original positions in the light field image.
- **Micro-Image Refilling** – Since most of the light field information is discarded when rendering the 2D views in the lower layers, this step aims at emulating the significant cross-correlation existing in light field content between neighboring micro-images so as to synthesize the missing texture samples as much as possible to complete the IL reference picture.

7.3 Mitigation of Packet Loss Impact on Scalable Light Field Coding

Guaranteeing successful light field video transmission in the presence of channel errors is a challenging issue that requires reliable error resilience mechanisms for fighting the transmission errors and mitigating their impact in the user quality perception.

State-of-the-art error resilience techniques for 2D and 3D multiview video can be typically categorized in three main groups [10]: i) error resilient encoding techniques, which are introduced into the video encoding process to make the bitstream more robust to errors; ii) error concealment techniques, which are employed at the decoding process to conceal the effect of errors; and, iii) those that require interactions between encoder and decoder to adaptively consider the network characteristics in terms of information loss [11, 12].

Since there is a lack of error resilience techniques specific for light field content, a simple error concealment technique is proposed to estimate the lost data making use of the inherent correlation existing in the light field content. In this section, a discussion about some of the relevant factors which affects the inter-layer prediction accuracy is firstly presented (in Section 7.3.1) and, then, the proposed error concealment method is defined (in Section 7.3.2).

7.3.1 Relevant Factors for the Inter-Layer Prediction Accuracy

Besides the aforementioned advantages of using a light field imaging system, it is important to notice that for representing the full light field in this type of content there is a massive increase in the amount of information that need to be captured, encoded and transmitted when compared to legacy technologies. As opposing the MVC approach where each enhancement layer represents an additional 2D view image, there is a considerable jump in the coding information amount between First and Second Enhancement Layers of the proposed scalable coding architecture.

To illustrate the relation between amounts of information in the lower hierarchical layers and the Second Enhancement Layer, consider one frame from the light field test image *Plane and Toy* (frame 123, in Fig. 7.2a), with resolution of 1920×1088 and micro-image resolution of around 28×28 pixels. From this light field content, 9 views are generated for the first two scalability layers– one for the Base Layer and eight for the First Enhancement Layer. These views are generated using the Basic Rendering algorithm with patch size of 4×4 and varying the position of the patch in relation to the center of the micro-image in {-8, -6, -4, -2, 0, 2, 4, 6, 8} pixels. Notice that, from this set of patch positions, adjacent patches contain overlapping areas of the micro-image. Consequently, approximately 12% of the information inside each micro-image is used to build these nine 2D views and the remainder data is discarded. The nine views are then coded independently with the High Efficiency Video Coding (HEVC) using the “Intra, main” configuration [13].

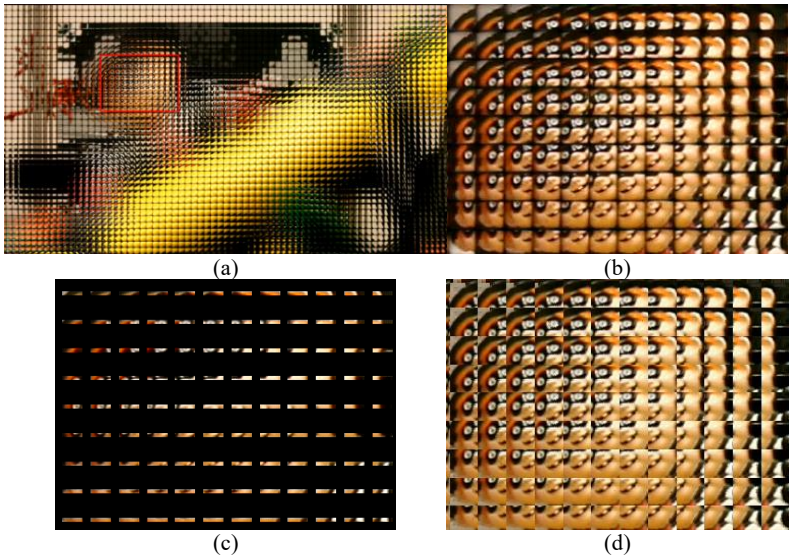

Fig. Error! Reference source not found.**.2** Light field image and corresponding IL picture prediction: (a) light field image Plane and Toy (frame 123); (b) Magnified section of 336×246 pixels from original image; (c) Magnified section of 336×246 pixels from sparse IL prediction picture; and (c) Magnified section of 336×246 pixels from full IL prediction picture.

Afterwards, the nine coded and reconstructed 2D views are processed to build an IL reference (see Fig. 7.1). In the Patch Remapping step, since there are overlapping areas between adjacent patches, this redundant information is used to refine the pixel values. The resulting sparse light field image is shown in Fig. 7.2b by the enlargement, to illustrate the amount of information that need to be estimated in the Micro-Image Refilling process. After this, by applying the Micro-Image Refilling process, the IL picture prediction is completed, as shown Fig. 7.2c. This IL picture prediction is then used as a new reference picture to efficiently encode the light field content in the Second Enhancement Layer (Section 7.2).

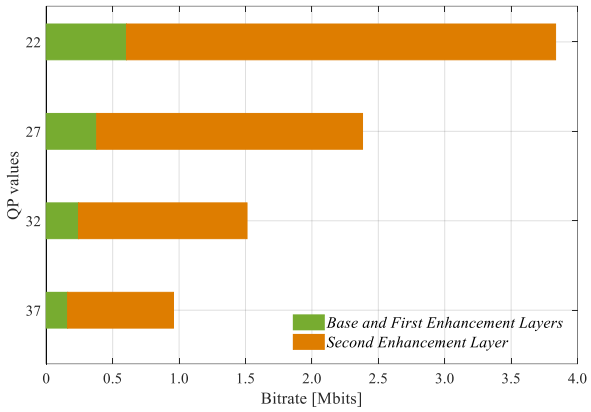

Fig. Error! Reference source not found.**.3** Relation between the amount of data in the bitstream for the Base Layer and First Enhancement Layer, compared to the Second Enhancement Layer.

Finally, in Fig. 7.3, the used bitrate for encoding all the nine 2D view images independently is compared to bitrate used to encode the light field content with the scalable coding scheme for four different Quantization Parameter (QP) values. From this, it can be seen that the Base Layer and the First Enhancement Layer represent only a small percentage of the scalable bitstream (in this case, about 16% of the scalable bitstream). Therefore, it is expected that losses in the lower hierarchical layers will considerably affect the accuracy of the built IL picture prediction and, consequently, degrade the performance of the proposed scalable coding scheme.

Moreover, it should be also noticed that, as was shown in [14], the performance of the inter-layer prediction scheme is improved when increasing the patches sizes. This fact is related again to the amount of data from a light field content that is discarded when generating a 2D view image and that need to be estimated in the Micro-Image Refilling process. As the amount of discarded information is a consequence of the chosen patch size and number of views, this means that the parameters which are freely chosen when generating the content in the lower hierarchical layers will also affect the accuracy of the build IL picture prediction.

Considering the Basic Rendering and Weighted Blending algorithms, these parameters are:

- **Patch Size** – During the creative post-production process, a proper patch size will be selected and will be limited to the used optical depth of field. As mentioned earlier, the quality of the IL picture prediction will improve as relative larger patch sizes are used.
- **Number and position of 2D views** – The choice of number of views and their corresponding positions is based on the type of display that will be used. In this case, as the number of 2D view images increases, less information from the light field content will be discarded and, consequently, the quality of the IL prediction

may improve. However, if these 2D views are generated by overlapping patches positions, the amount of relevant information to build the IL prediction picture is smaller, and its performance may decrease.

In other words, there is a large degree of freedom when defining how the light field content will be presented. Therefore, the error resilience problem need to be analyzed considering the parameters that control the generation of content for the lower hierarchical layers, since the quality of the inter-layer prediction is also dependent on them and may also affect the effectiveness of a resilience error technique.

7.3.2 Proposed Error Concealment Algorithm

Typically, an error concealment algorithm makes use of spatial, temporal, and spectral redundancy of the content to estimate the missing data and mask the effect of channel errors at the decoder.

Although the conventional error concealment tools for the lower layers in the hierarchical scalable architecture can be applied to the Second Enhancement Layer, these methods do not consider the inter-layer correlation between the multiview and light field content, and neither the inherent spatial correlation of the light field content.

When generating the IL picture prediction, the Micro-Image Refilling process is already able to estimate non-existing data to fill the holes in the IL picture prediction, by making use of the significant cross-correlation existing between neighboring micro-images. Therefore, considering that a 2D view image is lost (see Fig. 7.1), the only difference when building the IL picture prediction is that there will be more holes to be fulfilled in the Micro-Image Refilling process. This means that, it is possible to simply derive the error concealment algorithm from the inter-layer prediction method.

Therefore, upon the detection of a lost picture, the following steps are considered by the proposed error concealment algorithm to build the IL picture prediction:

i) The Patch Remapping process is employed considering only the set of 2D view images that are available (without loss). To illustrate the consequence of a lost 2D view in this step, five non-overlapping patch positions ({-8, -4, 0, 4, 8}) are used to generate five corresponding 2D view images from the light field image *Plane and Toy (frame 123)*. Then, considering that the central 2D view image (with patch position “0”) is not available at the decoder side, the sparse IL picture prediction will contain extra holes where the patches of the lost 2D view were supposed to be placed, as illustrated in a. Fig. 7.4a.

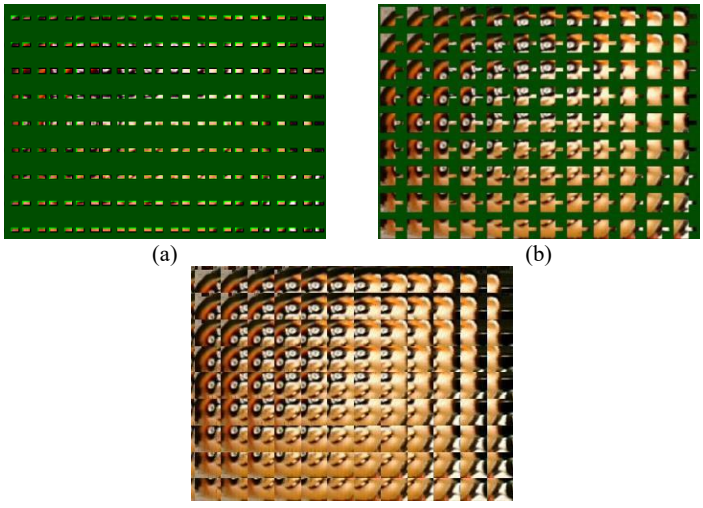

(a) (b)

(c)

Fig. Error! Reference source not found.**.4** Some steps of the used error concealment algorithm to build the IL reference when one 2D view image is lost: (a) The *Patch Remapping* for the available 2D view images; (b) One of the iterations of the *Micro-Image Refilling* to illustrate the recovery of the lost patches; and (c) The built IL picture prediction.

ii) The Micro-Image Refilling algorithm can estimate most of the holes by using information from available patch positions, including the set of lost patches in the position "0". This is illustrated in one of the steps of the algorithm (for the first 2D view) in Fig. 7.4b. Finally, it is possible to re-call the algorithm also for the lost patch position to fulfill the IL prediction picture, as shown in Fig. 7.4c.

7.4 Experimental Results

To properly analyze the influence of packet losses on the accuracy of the Inter-Layer prediction, the following test conditions were considered:

- **Light field test images** – Four light field images with different spatial and micro-image resolutions (MI_{resol}) are considered to achieve a set of representative results. These are (see Fig. 7.5): *Plane and Toy* (frames 23 and 123 from a sequence with identical name); *Robot 3D*; and *Laura*. The first three images are available in [15] and the last light field image in [16].

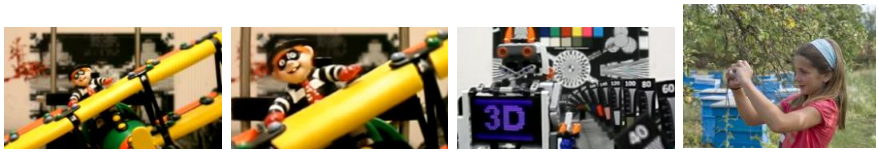

(a) *Plane and Toy (frame 23)* 1904×1064 $MI_{resol} = 28 \times 28$

(b) *Plane and Toy (frame 123)* 1904×1064 $MI_{resol} = 28 \times 28$

(c) *Robot 3D* 1904×1064 $MI_{resol} = 28 \times 28$

(d) *Laura* 7104×5328 $MI_{resol} = 74 \times 74$

Fig. Error! Reference source not found.**.5** Example of a central view rendered from each light field test image (with the corresponding characteristics below each image).

Table Error! Reference source not found.**.1** Test Conditions – Patch sizes and positions (in pixels) for generating content for the lower hierarchical layers (for each light field test image in Fig. Error! Reference source not found.**.5**)

Test Image	Patch Sizes	Patch Positions (Horizontal Positions)
Plane and Toy (frame 23)	{4 (in focus), 9, 11}	9 views: {-8, -6, -4, -2, 0, 2, 4, 6, 8} 5 views: {-8, -4, 0, 4, 8}
Plane and Toy (frame 123)	{4, 9(in focus), 11}	9 views: {-8, -6, -4, -2, 0, 2, 4, 6, 8} 5 views: {-8, -4, 0, 4, 8}
Robot 3D	{4 (in focus), 9, 11}	9 views: {-8, -6, -4, -2, 0, 2, 4, 6, 8} 5 views: {-8, -4, 0, 4, 8}
Laura	{7, 10 (in focus), 14}	9 views: {-28, -21, -14, -7, 0, 7, 14, 21, 28}

- **Hierarchical Content Generation** - To generate the content for the first two scalability layers, the four test images were processed with the Basic Rendering and Weighted Blending algorithms, proposed in [9]. In this process, nine 2D view images were generated – one for the Base Layer and eight for the First Enhancement Layer. Since the resolution of the micro-images varies from one image to another, the patch positions to generated 2D view images were chosen to have nine regularly spaced views within the micro-image limits. Additionally, three different patch sizes were chosen for each test image, which correspond to cases where adjacent patches are taken with and without overlapping areas. One of these patch sizes represents the case where the main object of the scene is in focus. Due to the small size of micro-images in *Plane and Toy* and *Robot 3D* images, an additional set of patch positions needed to be considered so as to have the case where the patches are taken without overlap areas. In this case, five regularly spaced 2D view images were generated.
- **Network Conditions** – It should be noticed that, due to the large number of possible combinations of test conditions (number of views, patch size and patch positions) and since this chapter is mainly focus on analyzing the influence of these parameters on the performance of the error concealment algorithm, it will not yet cover an extensive set of network conditions, which will be, however, considered in future work. To simulate the network conditions, it is considered that an entire 2D view image is coded into only one packet. Hence, loss of a packet implies

that the entire 2D view image must be recovered by the error concealment algorithm. Three different packet loss conditions were considered, where one, two and three packets are lost. Additionally, packet losses were assumed independent and identically distributed for all 2D view images. For this, it is considered a case where the two lower layers are independently encoded, since an enhancement layer would not be decodable if the 2D view image in the base layer was lost.

- **Results Analysis** – The results are presented in terms of the average Mean Squared Error (MSE) (for all the combination of lost 2D view images) of the IL picture prediction built by the error concealment algorithm, compared with the IL prediction picture when there is no packet loss. Alternatively, the average MSE is also shown discarding the cases where the first or the last pictures are lost, since when this happens, portion of the information cannot be recovered by the *Micro-Image Refilling* algorithm in the border of the IL picture reference.

The experimental results for each tested light field image can be seen in Figs. 7.6 to 7.12. In each Figs. (7.6 to 7.12), these results are split in different charts for each used rendering algorithm (Basic Rendering and Weight Blending algorithms) and for each patch size. Finally, each chart shows the corresponding average MSE value for all the possible combinations of lost 2D views (referred to as All Views) as well as the average MSE value when discarding the cases where the first or the last pictures are lost (referred to as Without Border Views). Additionally, the maximum and minimum MSE values in each case are also presented by the error bars.

Based on these charts, the following conclusions can be drawn in terms of:

- **Number of lost 2D view images** – This analysis compares how the accuracy of the built IL picture prediction varies when different numbers of 2D view images are lost. As expected, in all test conditions, the accuracy of the inter-layer prediction degrades as the number of lost views increases. For instance, considering the tested image *Laura* when using the larger patch size (14) to generate the 9 views with the Basic Rendering algorithm (in Fig. 7.12a), the average MSE value goes from 65.23, when only one view is lost, to 253.75, when three views are lost. Moreover, it can be seen that the influence of lost views is stronger when the first or the last 2D views are lost. For example, for the same abovementioned test condition, the corresponding average MSE values for the Without Border Views case are considerably smaller (respectively, 5.9 and 61.63 when one or three views are lost).
- **Different Patch Sizes** – This analysis compares the results when using different patch sizes, for each tested image with the same patch positions and rendering algorithms. Surprisingly, for all results, the patch size corresponding to the case where the main object is in focus was shown to be the less affected by lost 2D views, even when it is the smaller one. For instance, consider the results shown in Fig. 7.8 for *Plane and Toy (frame 123)*, where 9 views where generated with the Basic Rendering algorithm. The patch size 4, where the main object is in focus, presented smaller average MSE values than the presented when using larger patch sizes. However, it is known that in this case (patch size 4), more information from the light field image was discarded from the original light field

image (when generating the 2D views) and need to be estimated in the *Micro-Image Refilling* process. From this, it can be concluded that, in a sequence where there is interest in varying the patch sizes from one frame to another (e.g., the *Plane and Toy* sequence), the impact of losses will be considerably lower, since the main object is maintained in focus (which is, most of the times, the case).

- **Different Rendering Algorithms** – This analysis compares the results when using one of the rendering algorithms, Basic Rendering (in Figs 7.6a to 7.12a) and Weighted Blending (in Figs. 7.6b to 7.12b), for each tested image and test conditions shown in Table 7.1. From this, it can be seen that the accuracy of the inter-layer prediction using the Weighted Blending algorithm are generally better than using the Basic Rendering algorithm when one or more views are lost. This can be explained by the high level of blur which is introduced by the weighted average in the Weighted Blending algorithm. Hence, the differences in these blurred images will be less evident than differences in images generated by the Basic Rendering algorithm.
- **Different Number of 2D View Images in Lower Layers** – This analysis compares the results when different numbers of 2D views are generated to the lower layers, using the same patch sizes and rendering algorithms. For this, the results using 5 and 9 views for *Plane and Toy (frame 23)* (in Figs. 7.6 and 7.7), *Plane and Toy (frame 123)* (in Figs. 7.8 and 7.9), and *Robot 3D* (in Figs. 7.10 and 7.11) are compared. As expected, by using less 2D view images in the lower layer, a loss of 2D view images will affect more drastically the accuracy of the built IL picture prediction. This can be understood since, when considering less views: i) more information from the original light field image is discarded to generate the 2D view images; and ii) a loss of a 2D view image represent a higher packet loss rate.

It is important to notice that, although for these tests it was considered that an entire 2D view image is coded into only one packet, the *Patch Remapping* and *Micro-Image Refilling* processes could easily be adapted to the case where the lost packets represent slices of 2D view images. Moreover, from the presented analysis, it was shown that, although the parameters of the scalable coding architecture somehow interfere on the performance of the error concealment algorithm, in some cases, the used error concealment algorithm is able to recover the IL picture prediction with negligible MSE value (e.g. when the *Weighted Blending* algorithm is used). However, it is also important to consider cases where the losses happen in the *Second Enhancement Layer* of the proposed scalable coding solution, since the information in this layer represents the largest percentage of the scalable bitstream (as shown in Section 7.3.1). Therefore, these cases will be considered in future work.

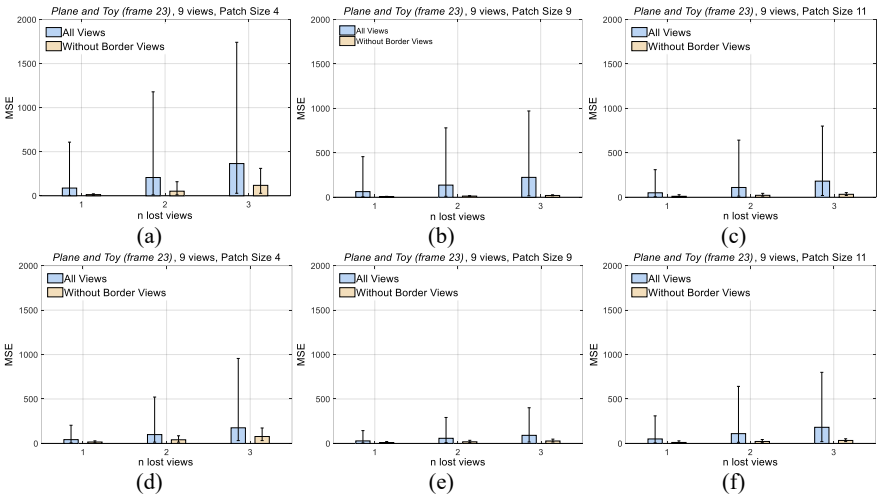

Fig. Error! Reference source not found..**6** Comparison between qualities of the IL reference when there are lost views. In this case, 9 views were generated with 3 different patches from the tested light field image *Plane and Toy (frame 23)* using: (a) Basic Rendering algorithm; and (b) Weighted Blending algorithm.

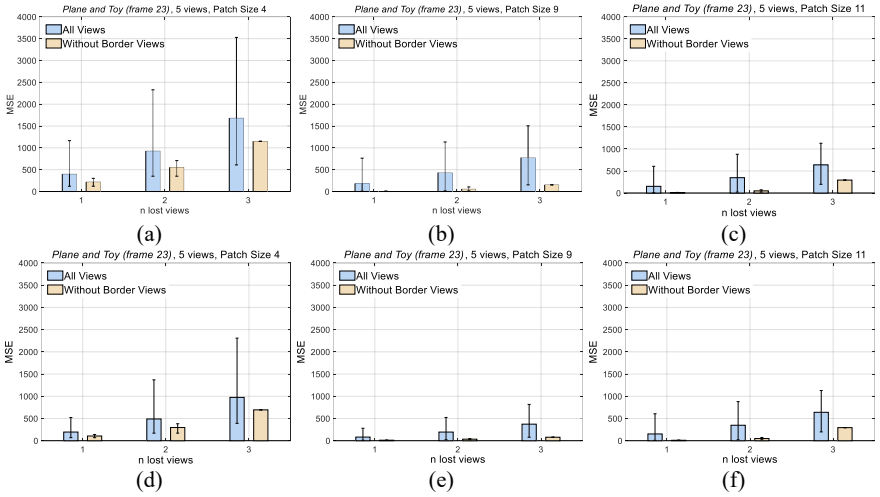

Fig. Error! Reference source not found..**7** Comparison between qualities of the IL reference when there are lost views. In this case, 5 views were generated with 3 different patches from the tested light field image *Plane and Toy (frame 23)* using: (a) Basic Rendering algorithm; and (b) Weighted Blending algorithm.

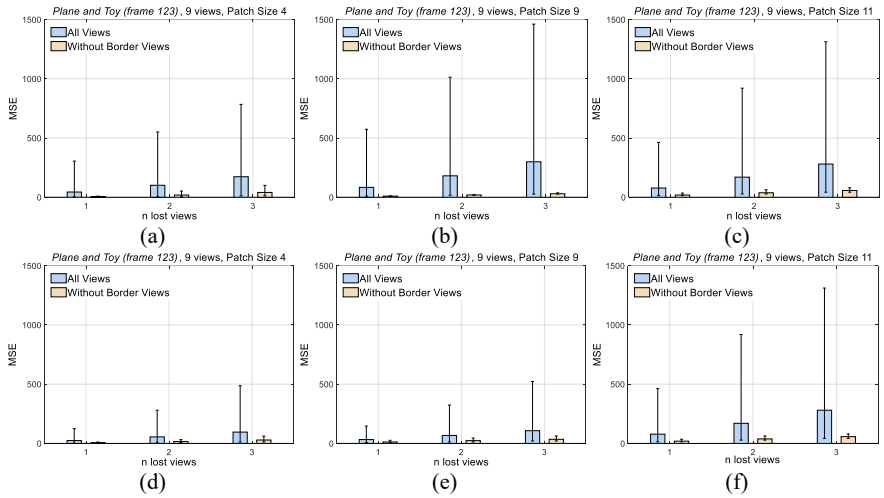

Fig. Error! Reference source not found.**.8** Comparison between qualities of the IL reference when there are lost views. In this case, 9 views were generated with 3 different patches from the tested light field image *Plane and Toy (frame 123)* using: (a) Basic Rendering algorithm; and (b) Weighted Blending algorithm.

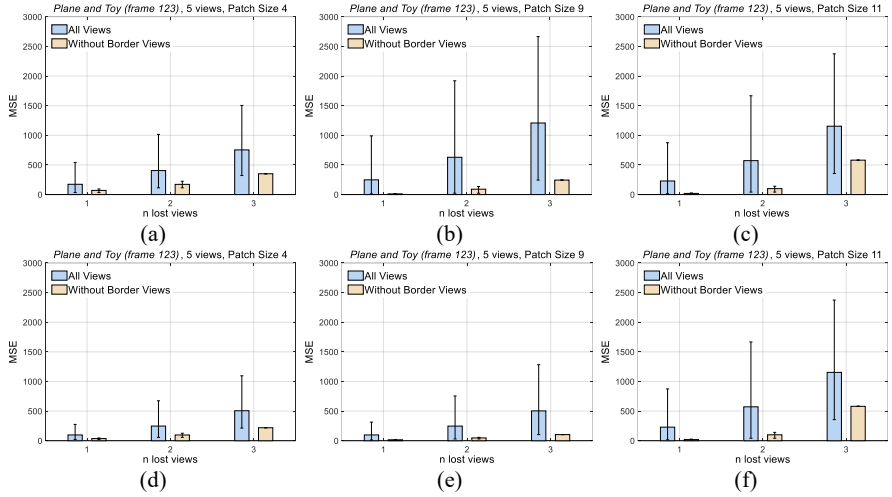

Fig. Error! Reference source not found.**.9** Comparison between qualities of the IL reference when there are lost views. In this case, 5 views were generated with 3 different patches from the tested light field image *Plane and Toy (frame 123)* using: (a) Basic Rendering algorithm; and (b) Weighted Blending algorithm.

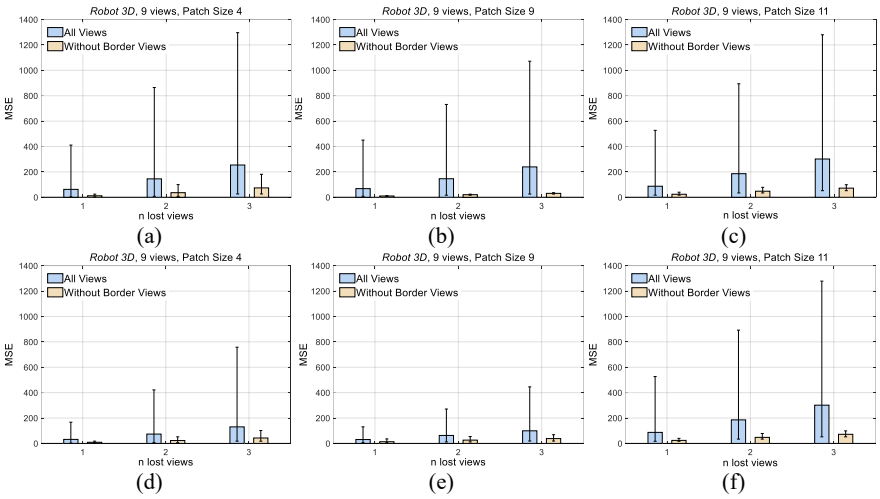

Fig. Error! Reference source not found.**.10** Comparison between qualities of the IL reference when there are lost views. In this case, 9 views were generated with 3 different patches from the tested light field image *Robot 3D* using: (a) Basic Rendering algorithm; and (b) Weighted Blending algorithm.

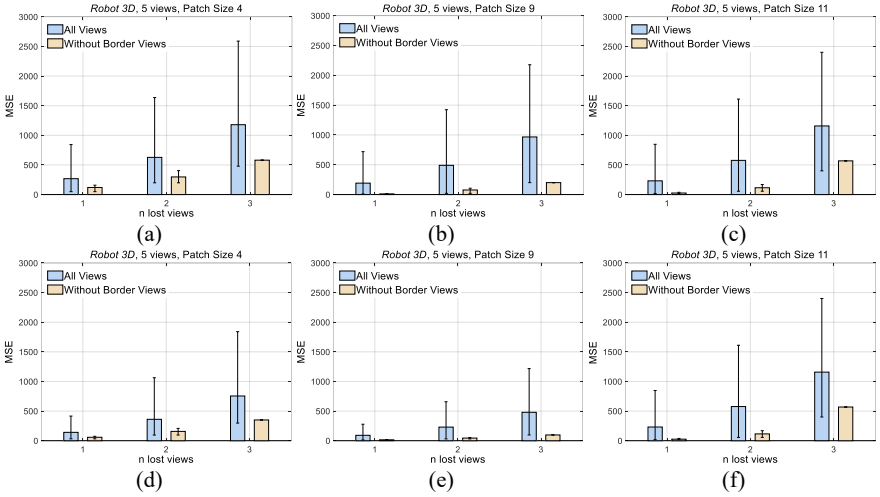

Fig. Error! Reference source not found.**.11** Comparison between qualities of the IL reference when there are lost views. In this case, 5 views were generated with 3 different patches from the tested light field image *Robot 3D* using: (a) Basic Rendering algorithm; and (b) Weighted Blending algorithm.

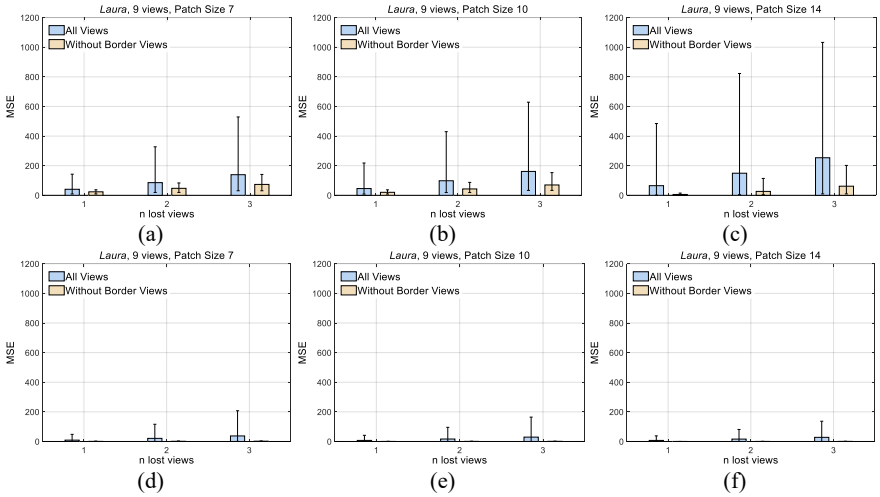

Fig. Error! Reference source not found.**.12** Comparison between qualities of the IL reference when there are lost views. In this case, 9 views were generated with 3 different patches from the tested light field image *Laura* using: (a) Basic Rendering algorithm; and (b) Weighted Blending algo-

7.5 Conclusions

This chapter proposed to start the discussion about error resilience techniques for light field content and presents a study of the influence of packet losses in display scalable light field content coding. For this, an error concealment algorithm was adopted to estimate the lost data, which was derived from the inter-layer prediction scheme previously proposed by the authors. From the presented study, it could be seen that although the parameters of the scalable coding architecture somehow interfere on the performance of the error concealment algorithm, in some cases, it is possible to recover the inter-layer prediction with negligible differences compared to the prediction when there are no losses. However, it is also important to consider cases where the losses happen in the Second Enhancement Layer of the proposed scalable coding solution. Therefore, future work includes proposal of error resilience techniques for dealing with transmission errors in this layer.

Acknowledgments This work was supported by FCT (*Fundação para a Ciência e a Tecnologia*, Portugal), under the project UID/EEA/50008/2013.

7.6 References

1. Raytrix (2012) Raytrix Website. http://www.raytrix.de/. Accessed 7 Jul 2014
2. (2012) Lytro Inc. https://www.lytro.com/. Accessed 7 Jul 2016
3. Georgiev T, Yu Z, Lumsdaine A, Goma S (2013) Lytro Camera Technology: Theory, Algorithms, Performance Analysis. In: Proc. SPIE 8667, Multimed. Content Mob. Devices. Burlingame, CA, US, p 86671J
4. Wang J, Xiao X, Hua H, Javidi B (2015) Augmented Reality 3D Displays With Micro Integral Imaging. J Disp Technol 11:889–893. doi: 10.1109/JDT.2014.2361147
5. Lanman D, Luebke D (2013) Near-Eye Light Field Displays. ACM SIGGRAPH 2013 Emerg Technol - SIGGRAPH '13 1–1. doi: 10.1145/2503368.2503379
6. Aggoun A, Tsekleves E, Swash MR, et al (2013) Immersive 3D Holoscopic Video System. IEEE Multimed 20:28–37. doi: 10.1109/MMUL.2012.42
7. (2016) Cisco Visual Networking Index: Global Mobile Data Traffic Forecast Update. 2015–2020 Cisco White Paper
8. Conti C, Nunes P, Soares LD (2014) Impact of Packet Losses in Scalable 3D Holoscopic Video Coding. In: Proc. SPIE Opt. Photonics, e Digit. Technol. Multimed. Appl. III. Brussels, Belgium, p 91380E
9. Georgiev T, Lumsdaine A (2010) Focused Plenoptic Camera and Rendering. J Electron Imaging 19:021106–021106. doi: 10.1117/1.3442712
10. Yao Wang, Wenger S, Jiantao Wen, Katsaggelos AK (2000) Error resilient video coding techniques. IEEE Signal Process Mag 17:61–82. doi: 10.1109/79.855913
11. Nunes P, Soares LD, Pereira F (2008) Error resilient macroblock rate control for H.264/AVC video coding. In: 2008 15th IEEE Int. Conf. Image Process. IEEE, pp 2132–2135
12. Nunes P, Soares LD, Pereira F (2009) Automatic and adaptive network-aware macroblock intra refresh for error-resilient H.264/AVC video coding. In: 2009 16th IEEE Int. Conf. Image Process. IEEE, pp 3073–3076
13. Bossen F (2013) Common HM Test Conditions and Software Reference Configurations. JCTVC-L1100, Geneva, Switzerland
14. Conti C, Nunes P, Soares LD (2013) Inter-Layer Prediction Scheme for Scalable 3-D Holoscopic Video Coding. IEEE Signal Process Lett 20:819–822. doi: 10.1109/LSP.2013.2267234
15. Geogiev T Todor Georgiev Gallery of Light Field Data. http://www.tgeorgiev.net/Gallery/. Accessed 17 Sep 2016
16. (2013) 3D Holoscopic Sequences (Download Link). http://3dholoscopicsequences.4shared.com/. Accessed 30 Oct 2016